Thermal conductivity of binary ceramic composites made of insulating and conducting materials comprising full composition range – Applied to yttria partially stabilized zirconia and molybdenum disilicide

Cernuschi, Federico; Kulczyk-Malecka, Justyna; Zhang, Xun; Nozahic, Franck; Estournès, Claude; Sloof, Willem G.

DOI
10.1016/j.jeurceramsoc.2023.06.059

Publication date
2023

Document Version
Final published version

Published in
Journal of the European Ceramic Society

Journal of the European Ceramic Society 43 (2023) 6296–6307

Contents lists available at ScienceDirect

Journal of the European Ceramic Society

journal homepage: www.elsevier.com/locate/jeurceramsoc

Thermal conductivity of binary ceramic composites made of insulating and conducting materials comprising full composition range – Applied to yttria partially stabilized zirconia and molybdenum disilicide

Federico Cernuschi [a], Justyna Kulczyk-Malecka [b,c], Xun Zhang [b], Franck Nozahic [d,e], Claude Estournès [d], Willem G. Sloof [f,*,1]

[a] RSE S.p.a., Via Rubattino 54, 20134 Milano, Italy
[b] School of Materials, The University of Manchester, M139PL, UK
[c] Surface Engineering Group, Manchester Metropolitan University, Manchester M15GD, UK
[d] CIRIMAT, Université de Toulouse, CNRS, INP-ENSIACET - 4 allée Emile Monso, Cedex 4 31030 Toulouse, France
[e] CIRIMAT, Université de Toulouse, CNRS, INPT, UPS, 118 Route de Narbonne, Cedex 9 31062 Toulouse, France
[f] Department of Materials Science and Engineering, Delft University of Technology, Mekelweg 2, 2628 CD Delft, the Netherlands

ARTICLE INFO

Keywords:
Thermal diffusivity
Thermal conductivity
Composites
Percolation
Thermal Barrier
Spark Plasma Sintering

ABSTRACT

The thermal diffusivity and conductivity of dense and porous binary composites having an insulating and conducting phase were studied across its entire composition range. Experimental evaluation has been performed with $MoSi_2$ particles embedded into yttria partially stabilized zirconia (YPSZ) as prepared by spark plasma sintering (SPS). The thermal diffusivity of the composites was measured with Flash Thermography (FT) and Laser Flash Analysis (LFA) techniques. Subsequently, the thermal conductivity was determined with the measured heat capacity and density of the composites. The actual volume fraction of the conducting phase of the composites was determined with image analysis of X-ray maps recorded with scanning electron microscopy (SEM). The phases present and their density were determined with X-ray diffractometry (XRD) using Rietveld refinement. The thermal diffusivity increases with increasing volume fraction of $MoSi_2$. Porosity reduces the thermal diffusivity, but the effect diminishes with high volume fractions $MoSi_2$. The thermal diffusivity as a function of the $MoSi_2$ volume fraction of the YPSZ composites is captured by modelling, which includes the porosity effect and the high conductivity paths due to the percolation of the conductive phase.

1. Introduction

Insulating materials used at high temperatures are chosen for their low thermal conductivity. These materials are often brittle ceramics, like alumina or zirconia. Strengthening or toughening of these materials by mixing in particles [1-3], which are conducting, affect their thermal conductivity [4,5].

Recently, particles, often conducting, were embedded into insulating ceramics to realize healing of crack damage [6-14]. At high temperatures in an oxidizing environment when the particles are intersected by a crack, they react with oxygen and the oxidation products filling the crack gap. This filling of the crack gap and wetting the crack faces may recover the composite strength and restore the component integrity [15, 16].

Understanding of the change of thermal conductivity or thermal diffusivity when an insulating material is mixed with a conducting material is of great interest for its applications. Predicting the properties of such a composite is paramount for their design [17].

In our preliminary study [4], inspired by self-healing thermal barrier coatings [6,7], the thermal conductivity or diffusivity of sintered composite samples consisting of $MoSi_2$ particles dispersed into a continuous yttria partially stabilized zirconia (YPSZ) matrix was carried out for $MoSi_2$ content up to 20 vol.%. In that study, different thermal conductivity models were examined and compared. From the various models already presented in the literature, the differential effective model (DEM) formulated by Bruggeman [18], and the semi-empirical model

* Corresponding author.
E-mail address: w.g.sloof@tudelft.nl (W.G. Sloof).
[1] +31 15 2784924

https://doi.org/10.1016/j.jeurceramsoc.2023.06.059
Received 19 November 2022; Received in revised form 28 April 2023; Accepted 23 June 2023
Available online 25 June 2023

developed by Nielsen [19,20], have been considered in particular. In addition, also a microstructure-based 2D finite element (FE) model was included.

Up to a volume fraction of 10% the experimental results were in good agreement with the Bruggeman model and the 2D FE model calculations. For higher volume fractions of $MoSi_2$, however, the experimentally determined thermal conduction increased significantly more than predicted by the Bruggeman and FE model. The Nielsen model represented the experimental data well when fitted with two parameters. Since this model is unable to predict thermal conductivity values for volume fractions greater than the parameter pertaining to the maximum packing of the dispersed species, it cannot be used for predicting thermal conductivity of composites with volume fractions of the dispersed species greater than 38%.

The aim of this work is to model the thermal conductivity of composites made of an insulating and conducting material across its entire composition range. To validate this model, two sets (dense and porous) of YPSZ composites with dispersed $MoSi_2$ particles comprising the full composition range were manufactured and studied.

2. Methods

2.1. Materials

Disc shaped YPSZ samples with various volume fractions of embedded $MoSi_2$ particles were prepared by Spark Plasma Sintering (SPS). The powder mixtures were produced by dry mixing yttria-partially stabilised zirconia containing 4 – 5 mol% Y_2O_3 (YPSZ, Amperit 827.774, H.C. Starck, Germany) with molybdenum disilicide ($MoSi_2$, 99.5% purity, ChemPur GmbH, Germany) using a Turbula mixer (Willy A. Bachofen AG Maschinenfabrik, Type T2C, Switzerland) with an equivalent mass of milling balls and powder during 12 h before densification.

2.2. Sample preparation

Prior to the SPS sintering process, the YPSZ powder was downsized from 40 to 7 μm using a planetary ball mill (Retsch PM 100, Germany). Zirconia balls of 10 mm diameter were used as grinding media. The ball to powder mass ratio was kept at 3:1. The rotor speed was 300 rpm and the milling time was 24 h. Also, the $MoSi_2$ powder was wind sifted to remove the fine fraction and the impurities. Wind sifting was performed using an Alpine 100 MRZ laboratory zig-zag classifier (Alpine Multi-Plex 100MRZ, Hosokawa Micron Powder System, Summit, New Jersey, USA). The airflow was fixed at 15 m^3/h and the classifier rotational speed was kept at 5000 rpm. The wind sifting resulted in a powder having an average diameter of 30 μm with a D10 and D90 value of 10 and 60 μm, respectively.

The particle size distribution of YPSZ and $MoSi_2$ powders was determined using a Malvern Master Sizer X laser diffraction instrument (Malvern Instruments Ltd., Worcestershire, UK). Prior to the measurements, the particles were ultrasonicated in deionized water (18.2 MΩ·cm at 25 °C) for 20 min.

A 15.4 mm inner diameter graphite die with a wall thickness of 12.3 mm was employed to sinter the composites in the SPS furnace (SPS-2080, SPS Syntex Inc., Kanagawa, Japan) located at the 'Plateforme Nationale de Frittage Flash' (PNF2, CNRS-CIRIMAT, Université de Toulouse, France). To prevent any possible reaction between the graphite die and the powders, a graphite foil 0.2 mm in thickness (PERMA-FOIL® Toyo Tanso, France) was placed between the punches and the powder as well as between the die and the powder. The powders were sintered in dynamic air vacuum (< 10 Pa) with a fixed heating rate of 100 °C/min. up to a soaking temperature in the range 1200–1600 °C, a soaking time in the range 5–20 min and a constant uni-axial pressure in the range 80–120 MPa depending on the desired final porosity. The temperature was monitored using an axial pyrometer focused on a small hole (3 mm in depth) located at the outer surface of the graphite die. The electric current was applied by a pulse following the standard 12:2 (on/off 3.3 ms) pulse pattern. Finally, after releasing the pressure, the graphite punches and die assembly was allowed cooling naturally from the sintering temperature to room temperature. Two batches of composites containing from nominally 10–75 vol.% of $MoSi_2$ were sintered. One batch concerning fully dense composites (porosity less than 4 vol.%) and the other batch porous composites (20 vol.% porosity on average). Pure YPSZ and $MoSi_2$ discs were also produced to serve as benchmark samples. The nominal porosity is equal to 100% minus the relative density, where the relative density is obtained from the ratio between the geometrical density and the theoretical density; cf. [21]. The geometrical density is determined from the weight and volume of the sample.

2.3. Characterisation

The microstructure of the samples was investigated by scanning electron microscopy (FEG-SEM, Quanta 650 and MIRA XMH, Tescan, Brno, Czech Republic), using backscatter electron (BSE) detector, energy dispersive X-ray spectroscopy (EDS, Oxford Instruments), and with 3D optical microscopy (Keyence, VHX Digital Microscope, Osaka, Japan). To this end,

the disc shaped samples were cut in half with a diamond wafering blade after thermal analysis; see Section 2.4. Next, to prepare cross sections, the specimens were impregnated in vacuum using epoxy resin. Thereafter, the surface was grinded and fine polished with diamond paste.

The specimen thickness has been evaluated as the average of 30 values measured by image analysis (IA) (Screen Measurement, Laboratory Imaging Ltd., Praha, Czech Republic) along the whole sample section.

The $MoSi_2$ content has been also evaluated by performing computerized image analysis (IA), using ImageJ software, of the binarized X-ray mapping of Mo as obtained by SEM-EDS analysis of selected sections of each sample. It was discovered that during the sintering process of the composite materials containing high volume fractions of embedded $MoSi_2$ rare, isolated silica particles were dispersed in the zirconia matrix alongside $MoSi_2$; see Fig. 1. As shown as an example in Fig. 1b these silica particulates could be detected under the EDS independently of $MoSi_2$, as Si-rich particles. Therefore, Si X-ray maps were considered less reliable than the Mo X-ray maps for determining the $MoSi_2$ volume fraction. The volume fraction pores (i.e., porosity) was determined from the binarized Zr and Mo X-ray maps representing the volume fraction of YPSZ and $MoSi_2$, respectively. Now, taking the porosity as the balance to accomplish 100% considering the sum of the as determined volume fractions of YPSZ and $MoSi_2$. These results agreed with backscattered electron images (BEI) taken along the sample cross-section.

Analysis of 10 images recorded with a magnification of 700x taken of the same sample showed that the uncertainty of the volume fraction $MoSi_2$ is less than 2% (absolute) and that of the volume fraction pores is within 0.5% (absolute) for the dense samples and within 2% (absolute) for the porous samples.

For a limited number of samples, the volume fraction $MoSi_2$ and the porosity has also been observed at higher magnification (1500x) to evaluate the effect of the magnification on the outcomes.

The geometrical characteristics of the porosity was evaluated by computerised image analysis (IA) using Avizo software.

Phase composition was analysed on both sample surface and section by X-ray diffraction (XRD, PANalytical X'Pert Pro (The Netherlands) and Oxford X'Calibur (UK)). As-received samples were scanned from 20.01 to 84.99 2θ° with 0.02 step size using Cu Kα radiation. Quantitative phase analysis based on Rietveld refinement method was then performed on patterns collected in the conventional Bragg - Brentano geometry (using Topas software or the GSAS-Expgui software). Lattice parameters were refined together, and the phase density were calculated

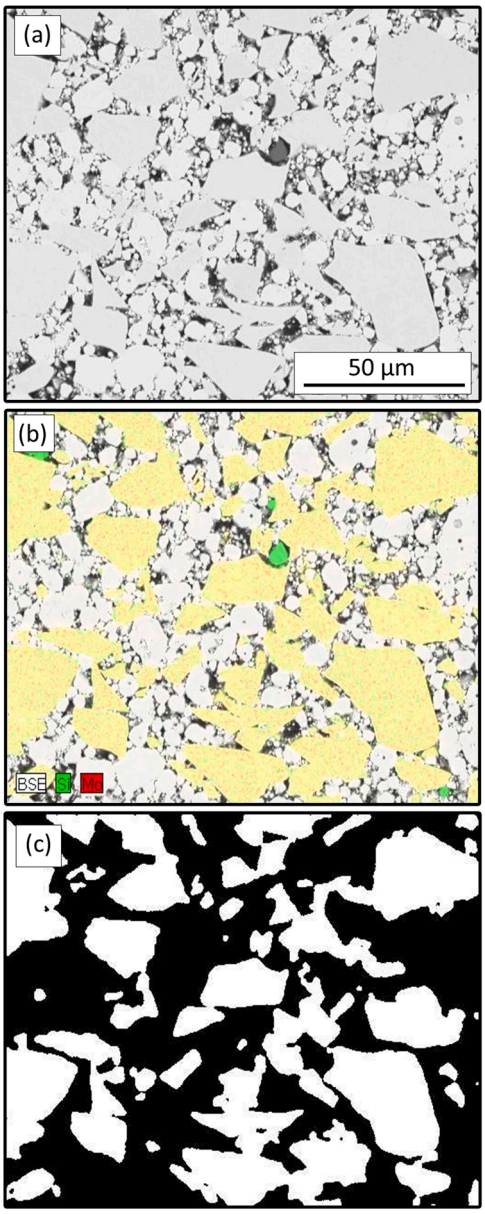

Fig. 1. Example of determining the volumetric fraction of $MoSi_2$ particles embedded into Yttria Partially Stabilized Zirconia (YPSZ) from scanning electron microscopy X-ray emission (EDS) mapping. (a) Backscattered electron image (BSE) image, (b) superposition of the Si and Mo X-ray emission maps on the BSE image, and (c) binarized image of the Mo X-ray emission map.

using known atomic positions [22]. From the series of XRD analysis of the YPSZ-$MoSi_2$ composites the variation of the density values was less than 0.2%.

2.4. Thermal analysis

The thermal diffusivity of both dense and porous samples was measured in air at room temperature by both Flash Thermography (FT) and Laser Flash Analysis (LFA) techniques [23-25]. For a selected set of samples, the thermal diffusivity was also measured as a function of temperature from room temperature up to 1200 °C in high vacuum (between 10^{-6} and 10^{-3} Pa) using a Laser Flash apparatus (Netzsch, LFA 427 and Theta Industries Inc., Port Washington, NY, USA).

Prior to analysis, samples were machined to discs of approximately 10 mm diameter and approximately 2 mm thickness. Owing to YPSZ translucency to the laser beam, a thin layers of graphite (Kontakt Chemie, Zele, Belgium) was painted on the surface of both sides of the sample, prior to evaluating the thermal diffusivity, to make the sample front face opaque to the Nd:YAG laser radiation (1060 nm) and to increase the rear face emissivity in the infrared (IR) detector sensitivity range; see for details Ref. [26].

During the measurements the entire front face of the sample was exposed quasi homogeneously to a short duration heat pulse (0.6 ms), which was supplied by a neodymium glass laser operated at 400 V. An InSb infrared detector cooled in liquid nitrogen was used to measure the temperature rise on the reverse side of the samples. Measurements were executed at various temperatures during the heating up procedure at approximately 100 °C intervals. Thermal diffusivity has been estimated from the experimental data of temperature versus time by using standard equations and methods accounting for finite pulse duration and heat losses [27,28]. These measurements were repeated five times in each condition. Typical accuracy for the LFA technique is 2–5% [24]. Here, conservatively 5% was taken.

Finally, the thermal conductivity values k were obtained from the density ρ_i and specific heat Cp_i of the constituting phases i and measured thermal diffusivity α using the following relationship:

$$k = \alpha \sum_{i=1}^{n} v_i \rho_i Cp_i \quad (1)$$

For which it holds that $\sum_{i=1}^{n} v_i = 1$; where n is the total number phases. The values used here for the density and specific heat capacity of YPSZ, $MoSi_2$ and air in the pores are summarized in Table 1. The values for the density of YPSZ and $MoSi_2$ are the average from XRD Rietveld refinement; see above. The specific heat capacity of YPSZ and $MoSi_2$ are taken from thermochemical data of pure substances [29], where for YPSZ Neumann-Kopp rule [30] was applied. These values are close to those reported from high accuracy differential scanning calorimetry (DSC); namely: 426.3 J/kg·K [31] for $MoSi_2$ and 458.8 J/kg·K for YPSZ [32]. The uncertainty of the values taken for the specific heat capacity of each phase is considered to be less than 1%. For the overall uncertainty of the as obtained thermal conductivity conservatively 10% was taken.

3. Results

3.1. Microstructure and composition of YPSZ-$MoSi_2$ composites

XRD analysis carried out on samples containing embedded $MoSi_2$ particles shows that these are composed of tetragonal YPSZ and tetragonal $MoSi_2$. The diffractograms in Fig. 2 show that there are no other crystalline phases present nor texture within any of the analysed samples.

Images collected from dense and porous SPS produced samples using digital optical microscope are shown in Fig. 3a-f. Dense and porous pure YPSZ are displayed in Fig. 3a and 3d, respectively. The porosity in the YPSZ matrix is visible as darker grey in Fig. 3d. The embedded $MoSi_2$ particles can also be distinguished easily from the YPSZ matrix due to their bright or white appearance. The porosity in the composite samples shown in Fig. 3e-f, can be recognized as darker patches in the light grey YPSZ matrix. There are no dark grey patches seen in the fully dense samples; see Fig. 3b and 3c. In these images, only $MoSi_2$ particles are visible as bright entities in the grey matrix of YPSZ. In both batches of dense and porous composites, however, increasing amounts of embedded particles can be observed. Percolated $MoSi_2$ particles (a

Table 1
Density ρ and specific heat capacity C_p of the three phases in the YPZ-$MoSi_2$ composite materials, at room temperature (298 K) and at 1 bar, used in calculations of thermal diffusivity and thermal conductivity; cf. Eq. (3).

Phase	Density, ρ (kg/m^3)	Specific Heat, C_p (J/kg•K)
YPSZ	6070 ± 12	454.6 ± 0.9
$MoSi_2$	6260 ± 13	426.3 ± 0.4
Air	1.161[46]	1016[46]

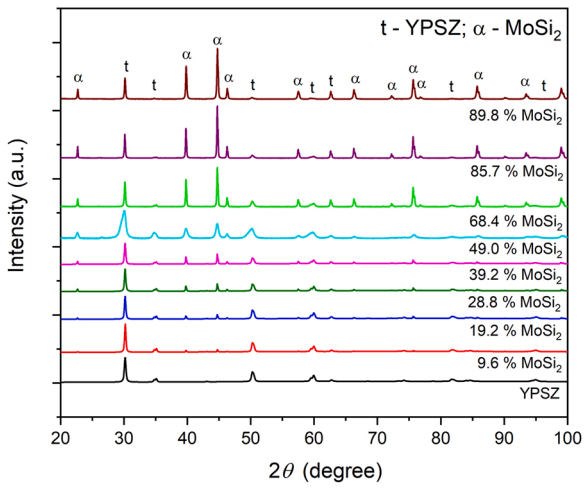

Fig. 2. X-ray diffractograms, recorded with Cu Kα radiation, of the Yttria Partially Stabilized Zirconia (YPSZ) composites with different volume fraction of $MoSi_2$. The diffraction lines of tetragonal YPSZ and tetragonal $MoSi_2$ are denoted.

phenomenon explained in the modelling section 4.2.1.) seem more apparent in samples containing more than 30 vol.% embedded $MoSi_2$ particles; see circled areas in images of Fig. 3c.

Polished surfaces of the SPS produced composite samples have been analysed with SEM in conjunction with X-ray microanalysis using EDS and digital optical microscope to characterise their microstructural features. Image analysis (IA) was conducted to determine the volume fraction of $MoSi_2$ and the volume fraction porosity; see Table 2. It is apparent that analytically obtained values differs slightly than the nominal composition of the samples. For porous samples, the differences in $MoSi_2$ volume fraction determined with IA compared to the nominal values depend on the fact that nominal values refer to the quantity of $MoSi_2$ particles mixed with YPSZ without considering the volume occupied by the porosity.

Examples of SEM backscattered electron images collected from a dense and porous composite containing 68.4 and 66.7 vol.% of embedded $MoSi_2$ particles into YPSZ, respectively, are shown in Fig. 4a and 4b. The binary images extracted from the BSE images show the porosity; see Fig. 4c and 4d. Since no apparent contrast between particles and the matrix is visible in the backscattered electron images, X-ray emission maps of Zr and Mo and Si were used to recognise the particles in the YPSZ matrix; see Fig. 4e-j. For the determination of the content of embedded $MoSi_2$ particles X-ray emission maps of Mo were used; see Fig. 4g-h.

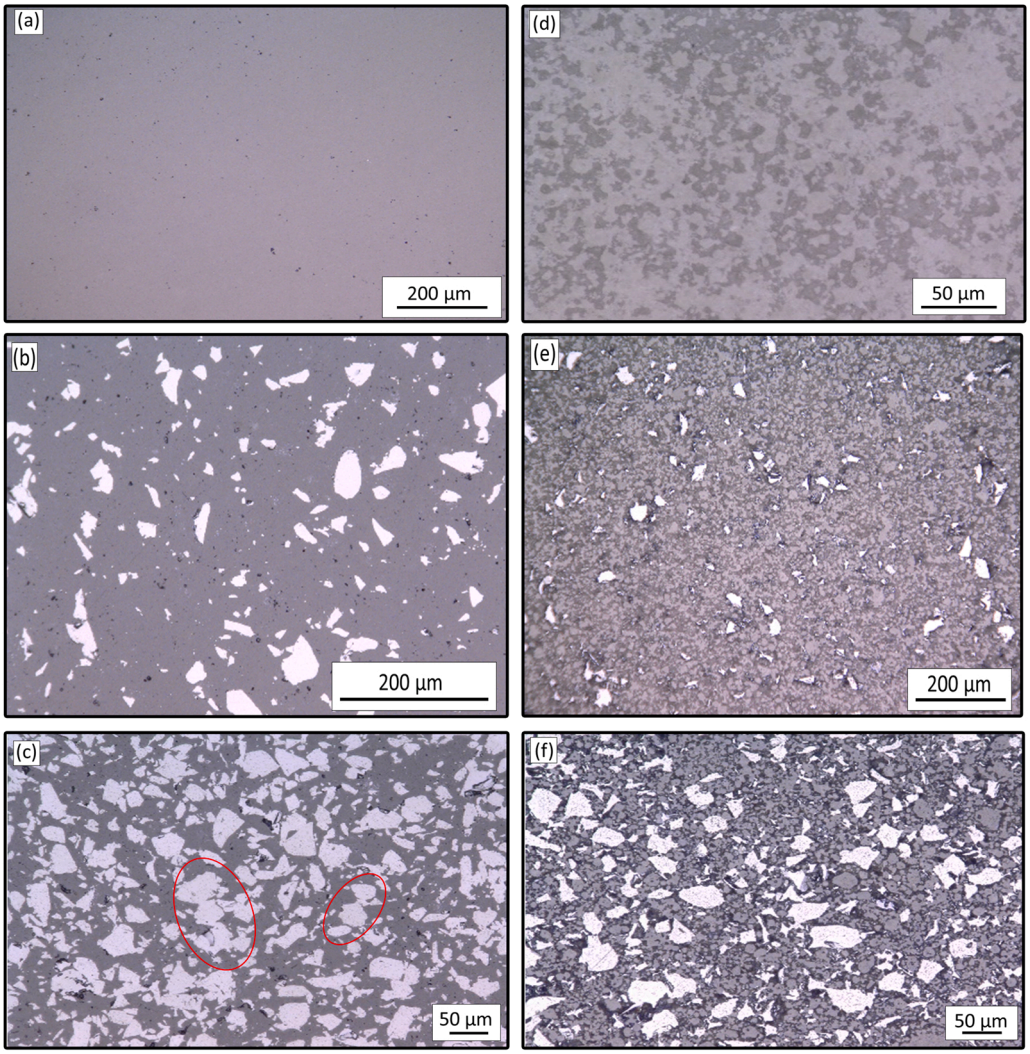

Fig. 3. 3D optical images collected from (a) dense and (d) porous pure Yttria Partially Stabilized Zirconia (YPSZ). Dense YPSZ composites with (b) 9.6 and (c) 39.2 vol.% $MoSi_2$. Porous YPSZ composites with (e) 7.7 and (f) 31.6 vol.% $MoSi_2$. The red markings in (c) indicates possible percolation of the $MoSi_2$ particles.

Table 2
Volume fraction of $MoSi_2$ and porosity of YPSZ-$MoSi_2$ composite materials as obtained from image analysis (IA) performed on images collected from SEM and EDS mapping (based on Mo map); see text for details. The uncertainty of the volume fraction $MoSi_2$ is within 2%; the uncertainty of the volume fraction pores of the dense composite is within 0.5% and of the porous composites within 2%.

Sample annotation*	Nominal volume fraction of $MoSi_2$ (%)	Volume fraction of $MoSi_2$ (%)	Porosity (%)
D-pure YPSZ	0	0	1.2
D-10%$MoSi_2$	10	9.6	3.6
D-20%$MoSi_2$	20	19.2	2.8
D-30%$MoSi_2$	30	28.8	2.6
D-40%$MoSi_2$	40	39.2	0.5
D-50%$MoSi_2$	50	49.0	3.2
D-60%$MoSi_2$	60	68.4	3.6
D-70%$MoSi_2$	70	85.7	3.2
D-75%$MoSi_2$	75	89.8	2.9
D-pure $MoSi_2$	100	97.2	2.8
P-pure YPSZ	0	0	12.0
P-10%$MoSi_2$	10	7.7	25.7
P-20%$MoSi_2$	20	15.4	26.1
P-30%$MoSi_2$	30	24.4	23.9
P-40%$MoSi_2$	40	31.6	23.5
P-50%$MoSi_2$	50	40.5	17.4
P-60%$MoSi_2$	60	63.7	12.7
P-70%$MoSi_2$	70	79.9	10.3

* D denotes dense, and P denotes porous composites.

In order to evaluate possible effect of the magnification on the estimated porosity and $MoSi_2$ content, measurements have been repeated on four samples at two different magnifications, viz.: 700 and 1500 times; see Fig. 5. Although, the statistics are limited (especially at higher magnification) values obtained at magnifications of 700 times have been confirmed and summarised in Table 3.

3.2. Thermal diffusivity and thermal conductivity of YPSZ-$MoSi_2$ composites

The thermal diffusivity and thermal conductivity at room temperature in air as a function of the volume fraction $MoSi_2$ embedded in porous and dense YPSZ are shown in Fig. 6a and 6b, respectively. As can be seen from these graphs, the thermal diffusivity and conductivity values are lower for porous composites. This is due to the fact that pores act as thermal insulation, as the thermal conductivity of air is only about 0.026 $Wm^{-1}K^{-1}$ at room temperature and decreases with increasing temperature, and is much lower than that of the YPSZ (2.0–2.8 $Wm^{-1}K^{-1}$ at room temperature) [33]. Furthermore, when the pore sizes are only a few orders of magnitude larger than the mean free path of gas molecules ($\cong$ 3.7 10^{-10} m), the gas thermal conductivity drops drastically to values that are one or two orders of magnitude smaller. Hence, this porosity related bottleneck effect on heat transfer is attributed to lower thermal diffusivity or conductivity values for the porous samples.

The thermal diffusivity and thermal conductivity of porous samples in air and vacuum at room temperature as a function of the volume fraction of $MoSi_2$ particulates is shown in Fig. 7a and 7b, respectively. These results allow to compare an effect of the atmosphere on heat transfer and thermal conductivity of the samples. Since the difference in both the thermal diffusivity and conductivity between samples analysed in air and vacuum is negligible, these properties of the samples are insensitive to change of the measurement environment. This suggests that the pores are closed or very small. In the latter, the Knudsen effect [34] (i.e., a drop in thermal conductivity of gases is seen when the mean free path of gas molecules is of the same order of magnitude as the pore size) reduces the thermal diffusivity measured in air to the same level as the thermal diffusivity measured in vacuum.

The thermal diffusivity and thermal conductivity of the dense samples measured in vacuum from room temperature up to 1200 °C with 100 °C intervals are shown in Fig. 8a and 8b, respectively. It can be seen that the thermal diffusivity reduces as the temperature increases reaching a plateau typical for YPSZ. It is also apparent that samples containing a higher volume fraction of $MoSi_2$ particles show the tendency to reduce thermal diffusivity as the temperature increases, which is a typical behaviour for $MoSi_2$. In Fig. 8b the estimated values of thermal conductivity according to Eq. (1) are plotted as a function of temperature. As the volume fraction of the particulates increases, the trend in thermal conductivity change rises with increasing temperature. The thermal conductivity of pure YPSZ is almost independent of temperature, while the thermal conductivity of $MoSi_2$ depends strongly on temperature. Moreover, as the volume fraction of the particulates increases, so is the overall thermal diffusivity or conductivity of the sample, which is again attributed to $MoSi_2$.

To confirm the tendency of increased thermal diffusivity or conductivity being attributed to the presence of $MoSi_2$ particles and lack of porosity, the thermal diffusivity versus temperature for samples containing different amounts of porosity (ranging from 1 to 22 vol.%) with and without $MoSi_2$ dispersion is presented in Fig. 9a. As expected, the thermal diffusivity of these samples decreases as much as the porosity increases for the two sets of samples, and the thermal diffusivity of samples with 16–20 vol.% $MoSi_2$ exhibit a higher thermal diffusivity compared with those made of only pure YPSZ; see Fig. 9b.

3.3. Modelling of thermal conductivity or thermal diffusivity

It is worth noting that when thermal properties of a heterogeneous material have to be modelled, the field parameter involved is thermal conductivity. Once thermal conductivity k_c of the composite is obtained, whatever the model used, the thermal diffusivity α of a composite made of n phases is estimated according to the definition of thermal diffusivity and the rule of mixture for the heat capacity (cf. Eq. (1)):

$$\alpha = k_c \Big/ \sum_{i=1}^{n} v_i \rho_i C p_i \tag{2}$$

As in several cases, the thermal conductivity or diffusivity of a composite media has been successfully simulated [26,35,36] by using the Bruggeman asymmetric model [18], also here this model has been applied. Furthermore, starting from the consideration that these composites consist of mixtures of two powders with distinct granulometric distributions and contain different levels of porosity, also the simple symmetrical Self-Consistent (SC) model [37] has been included in the analysis.

For a medium consisting of a continuous matrix (here YPSZ) and a dispersion of particles (here $MoSi_2$ or pores), it is assumed in the Bruggeman model that the particles are mainly surrounded by the matrix. When the granulometric distribution is not self-similar [38] over wide dimensional scales, this assumption is reasonably true only for low volumetric fraction of dispersions.

According to Bruggeman model, the thermal conductivity k of a two-phase asymmetric medium containing a volumetric fraction f of dispersed spheroids with thermal conductivity k_d embedded in a matrix with thermal conductivity k_m can be estimated as:

$$(1-f) = \left(\frac{k_m}{k}\right)^{\zeta} \frac{k_d - k}{k_d - k_m} \left(\frac{k + \gamma k_d}{k_m + \gamma k_d}\right)^{\eta} \tag{3}$$

Where ζ, γ and η are related to the relative orientation between thermal flux and the shape of dispersed particles.

The SC model can be used for simulating the thermal conductivity of symmetrical cell materials that possess phase inversion symmetry. According to Torquato [37], this means that for a two-phase material the morphology of phase 1 at volume fraction φ_1 is statistically identical to that of phase 2 when the volume fraction of phase 1 is equal to $1\text{-}\varphi_1$.

Among the effective medium approximations available in the literature, the self-consistent approximation for a symmetrical material [38-40] consisting of M different phases with volumetric fractions $\varphi_1 . \varphi_M$

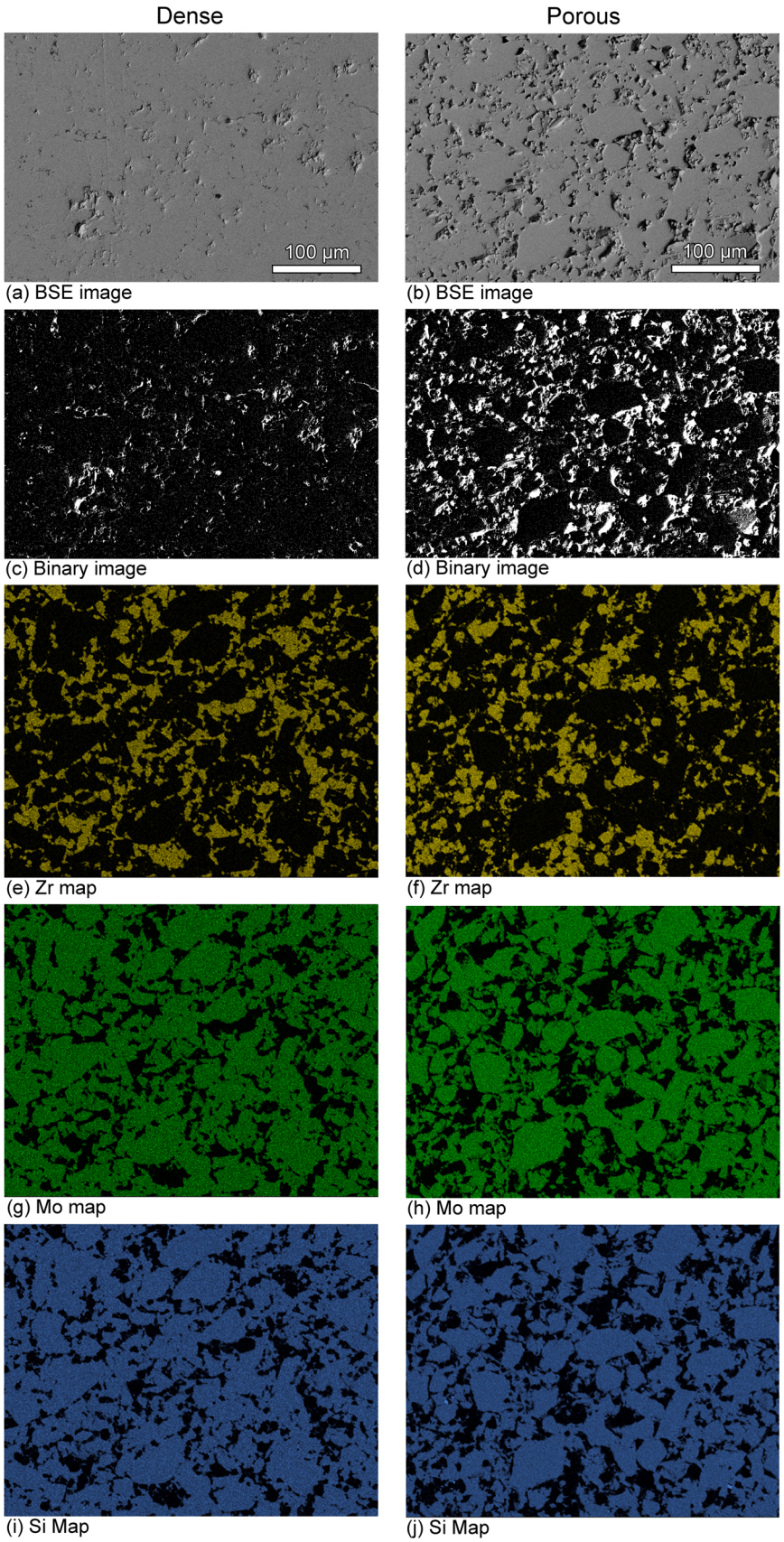

Fig. 4. (a) and (b) Scanning electron microscopy backscattered electron images collected from dense and porous Yttria Partially Stabilized Zirconia (YPSZ) composites with 68.4 and 66.7 vol.% embedded $MoSi_2$ particles, respectively. (c) and (d) Binary images showing the porosity. (e) and (f) Zr X-ray emission (EDS) maps. (g) and (h) Mo maps, and (i) Si and (j) Si maps.

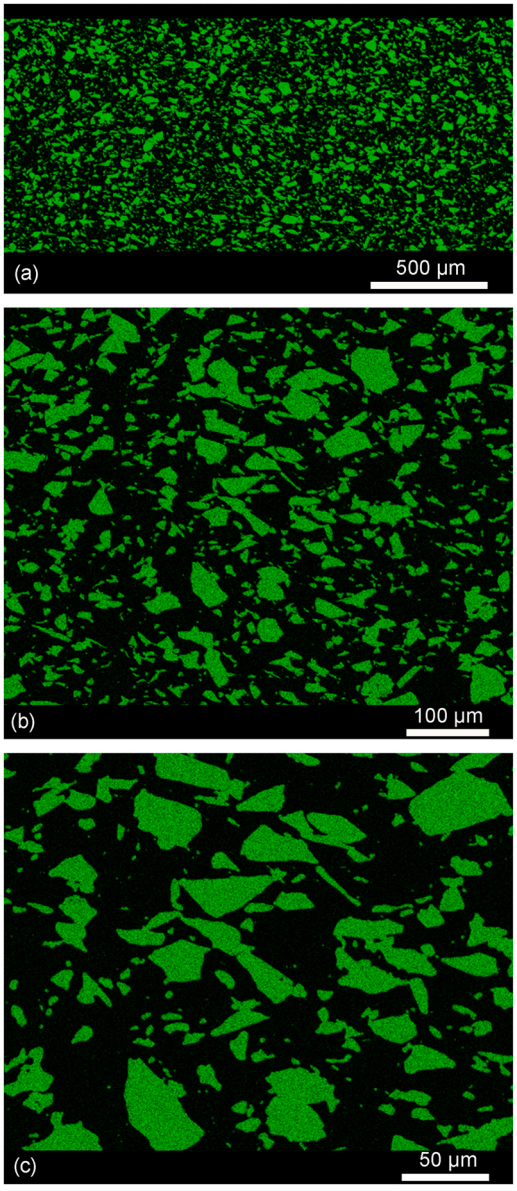

Fig. 5. Scanning electron microscopy X-ray emission (EDS) maps of Mo collected from dense Yttria Partially Stabilized Zirconia (YPSZ) composite with 28.8 vol.% embedded $MoSi_2$ particles at three different magnifications showing a practically self-similar microstructure; viz.: (a) 200x, (b) 700x and (c) 1500x.

and thermal conductivities $k_1.k_M$ can be easily applied when only spherical inclusions are considered. Then, the effective conductivity k_e can be estimated by solving the following equation [29]:

$$\sum_{j=1}^{M} \varphi_j \frac{k_j - k_e}{k_j - (d-1)k_e} = 0 \tag{4}$$

Where d is the space dimension, which in our case equals 3. It is noted that a more general expressions for ellipsoidal inclusions can be found in Ref. [37].

To make such a type of material feasible, the particle size distribution should be within some orders of magnitude to guarantee the self-similarity at different length scales [38]. Since the particle size distribution in the YPSZ-$MoSi_2$ composites does not range over several orders

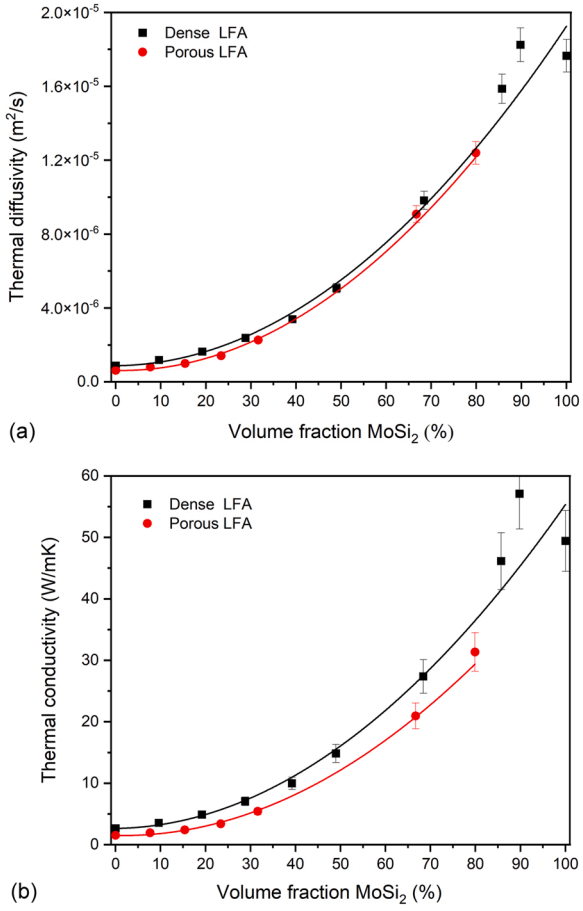

Fig. 6. (a) Thermal diffusivity measured and (b) thermal conductivity estimated as a function of the volume fraction of embedded $MoSi_2$ particles into dense and porous Yttria Partially Stabilized Zirconia (YPSZ) at room temperature in air.

Table 3
Volume fraction $MoSi_2$ and porosity of selected YPSZ-$MoSi_2$ composite materials as determined from image analysis (IA) performed on images collected from SEM and EDS mapping (based on Mo map) at two magnifications; uncertainty less than 2% (absolute).

Sample annotation*	Magnification (-)	Number of images (-)	Porosity (%)	Nominal porosity (%)	$MoSi_2$ (%)	Nominal $MoSi_2$ (%)
P-20%$MoSi_2$	700x	5	26.1	20	15.4	20
	1500x	2	29.2	20	17.3	20
P-30%$MoSi_2$	700x	3	23.9	22	24.4	30
	1500x	2	25.8	22	24.7	30
P-40%$MoSi_2$	700x	3	23.5	21	31.6	40
	1500x	2	26.0	21	34.7	40
P-50%$MoSi_2$	700x	3	17.4	19	40.5	50
	1500x	6	19.0	19	44.3	50

* P denotes porous composites.

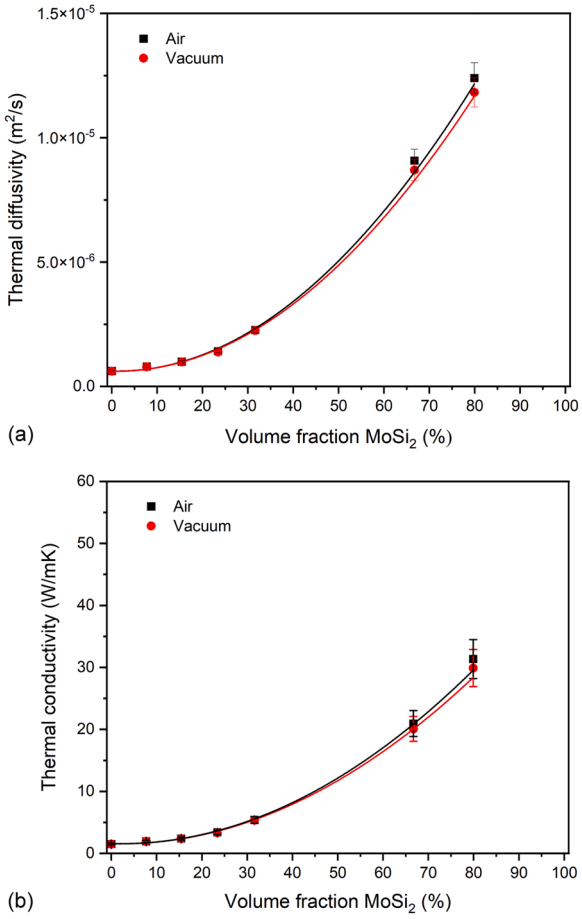

Fig. 7. (a) Thermal diffusivity measured and (b) thermal conductivity estimated as a function of the volume fraction of embedded $MoSi_2$ particles into porous Yttria Partially Stabilized Zirconia (YPSZ) at room temperature in air and vacuum.

of magnitudes, it is assumed that the particles are distributed widely enough to model the composites like a symmetrical cell matter.

3.4. Predictions and comparison with experimental data

For both dense and porous composites, samples consist of a three-phases mixture: YPSZ, $MoSi_2$ and pores. In the case of the Bruggeman model, the mixing of the three phases requires an iterative process. As a first step, the second phase is dispersed into the matrix (first phase) and in a subsequent step the third phase is added to the two-phase composite, which is considered as the continuous matrix. Since the outcome of the model must be independent from the mixing procedure, the final value for the thermal conductivity is taken as an average from the thermal conductivity values obtained by permuting the mixing order of the two dispersions inside the matrix.

In the SC model, on the contrary, the three phases are mixed in a single step according to Eq. (4). The particle shape is supposed to be spherical for each phase (i.e., YPSZ, $MoSi_2$ and pores) in the modelling of the composite's thermal conductivity. As observed, the YPSZ and $MoSi_2$ particles, and the pores (both for dense and porous samples) show a morphology not differing much from a spherical shape; see Fig. 10. From image analysis, more than 95% of the volume fraction of particles and pores are spheroids with elongation values e smaller than 3.2. It is noted that, according to the Bruggeman modelling, the thermal conductivity of a medium with either 60 vol.% of $MoSi_2$ or pores dispersed in a matrix of YPSZ varies less than 10% when comparing the case where all particles or pores are spherical (i.e., e equals 1) with the case that all these spheroidal dispersions are having an elongation e equal to 3.2. Moreover, spherical pores reduce the thermal conductivity less than spheroids, while for $MoSi_2$ particles the opposite holds [24].

The results of the calculations according to both the Bruggeman and SC model, for both dense and porous samples, and using input parameters summarised in Table 1, are shown in Fig. 11. In order to consider that inside micrometric pores the thermal conductivity of air is significantly reduced, because of the Knudsen effect [41] (cf. Section 3.2), only half of the thermal conductivity of 'bulk' air (i.e., k equals 0.026 W/mK) has been taken into account. Furthermore, in agreement with the experimental results, a porosity content of 3 and 20 vol.% have been considered in the modelling for dense and porous samples, respectively.

As in our previous work [4], also the inverse case of the Bruggeman model (denoted as Bruggeman II) was considered, i.e., composites with a continuous $MoSi_2$ matrix and a dispersion of YPSZ and pores. In addition, also a so-called 1D in-parallel model [29] has been included representing the upper bound for thermal conductivity or diffusivity of

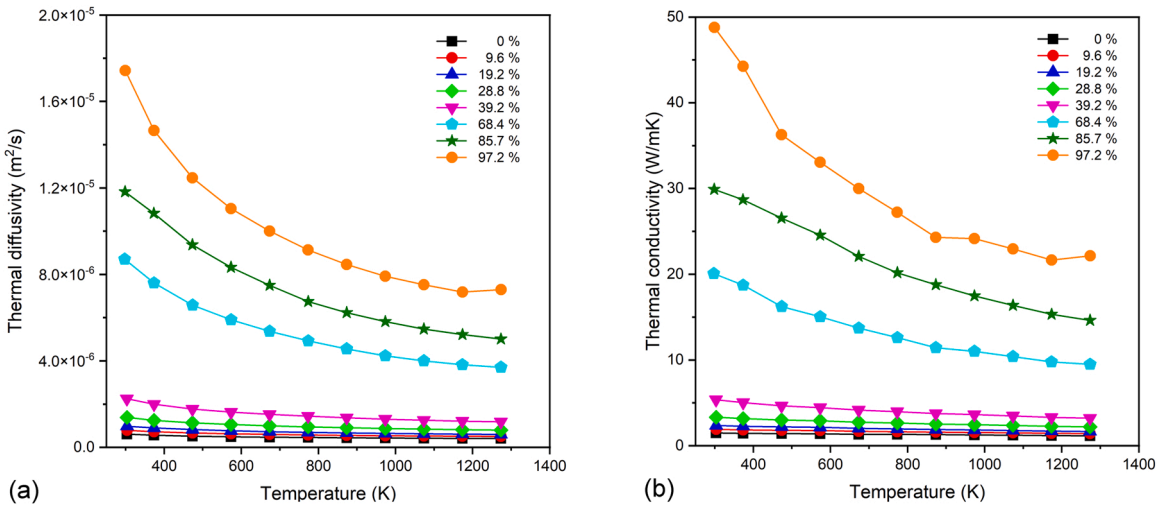

Fig. 8. (a) Thermal diffusivity measured and (b) thermal conductivity estimated of dense Yttria Partially Stabilized Zirconia (YPSZ), pure $MoSi_2$ and dense YPSZ-$MoSi_2$ composites as a function of temperature measured in a vacuum.

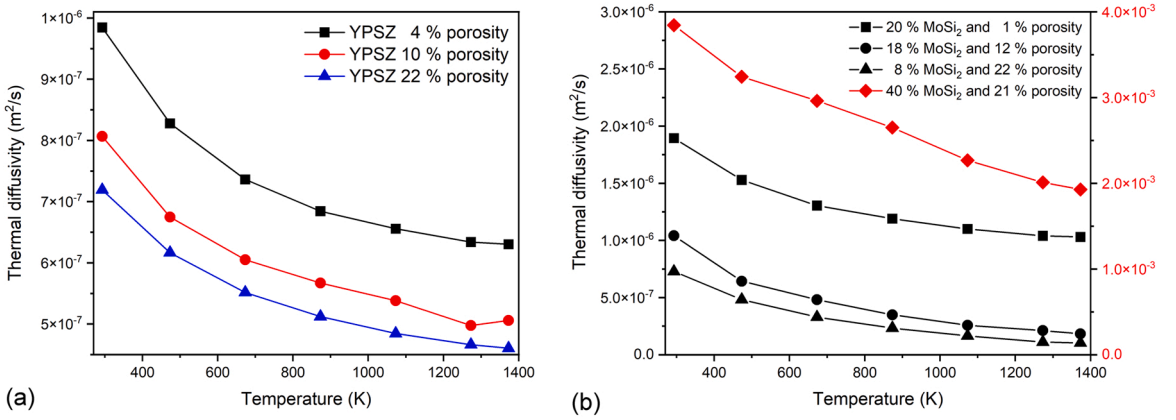

Fig. 9. (a) The effect of different porosity content of YPSZ on the thermal diffusivity as a function of temperature. (b) The effect of different volume fractions of $MoSi_2$ embedded into YPSZ on the thermal diffusivity as a function of temperature.

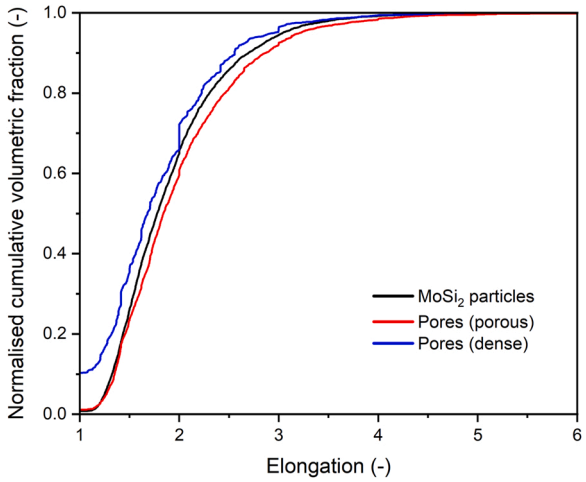

Fig. 10. Normalised cumulative volumetric fraction of embedded $MoSi_2$ particles and pores versus their elongation. Note that more than 95% of the volumetric fraction of either particles or pores has an elongation smaller than 3.2.

composites; see Fig. 11.

4. Discussion

4.1. Dense YPSZ-$MoSi_2$ composites

The Bruggeman model I (YPSZ matrix) predicts correctly the experimental data only for $MoSi_2$ volumetric fractions less than 30%; see Fig. 11a. For higher $MoSi_2$ volume fractions, the experimental data lay between the curves of the Bruggeman I and Bruggeman II model. This indicates that some high conductivity paths through the sample thickness occurred.

The Bruggeman II model provides thermal diffusivity values significantly higher than either those observed experimentally (apart from those composites with a very high $MoSi_2$ volume fraction) or predicted by Bruggeman I model; see Fig. 11a. This is attributed to the assumed continuous high conductive matrix and the presence of thermal percolation paths [42] even at low volume fractions of $MoSi_2$. Thus, the Bruggeman II model describes a much more effective transmission of heat through the thickness of the composite than described by the Bruggeman I model.

Moreover, for low contents of $MoSi_2$, the Bruggeman II model postulates the existence of a continuous highly conductive matrix,

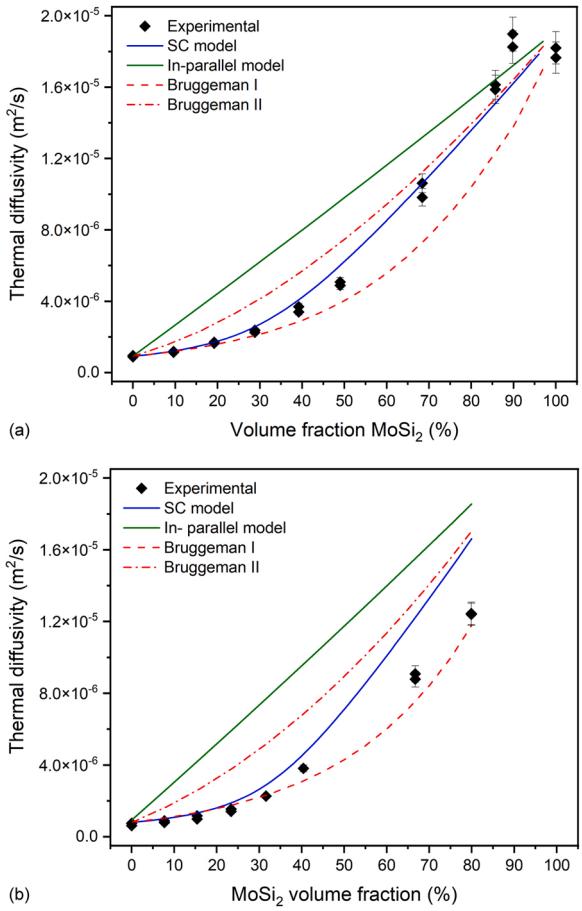

Fig. 11. Thermal diffusivity of (a) dense and (b) porous Yttria Partially Stabilized Zirconia (YPSZ) composites versus the actual volume fraction of embedded $MoSi_2$ particles compared with predictions according to the self-consistent, 1D in-parallel and Bruggeman I and II models; see text for details.

suggesting the presence of thermal percolation paths. Although less effective than in the 1D in-parallel configuration (the upper bound for the thermal modelling), the thermal percolation paths described by the Bruggeman II model are more effective in transmitting the heat through the thickness of composites than by both the Bruggeman I and the SC model for intermediate $MoSi_2$ volumetric contents.

The deviation between the experimental thermal diffusivity for high volumetric fractions of $MoSi_2$ particles and the prediction by the

Bruggeman I model is supposed to be related to the self-similarity hypothesis [38]. Nevertheless, this model does abolish the maximum filling or packing factor [43] limiting the volume fraction of the dispersion to a values smaller than 100%, which is seen in several other models proposed in the literature, such as the Nielsen model [19] for example.

The self-similarity over a wide length scale requires having the same dispersion of particles into the continuous matrix at different length scales [38]. This means that at every magnification the microstructure of these composites appears the same and consists of a dispersion of particles each surrounded by a continuous matrix. Then, the occurrence of 3D percolation paths through the composite thickness may be limited by this self-similar microstructure where the less conductive matrix is always present and limits the effectiveness of the direct contact between the highly conductive particles.

In reality, the dense composite does not fully meet the self-similarity hypothesis. When the volume fraction of highly conductive $MoSi_2$ particles exceeds a certain value, i.e., about more than 30%, then the number of high conductivity paths through the composite thickness increases more rapidly, and therefore the model is more effective than the SC model, which considers an ideal self-similar medium. This percolation phenomenon can be confirmed by looking at the microstructure of the dense composite with 39.2 vol.% $MoSi_2$; see Fig. 3c. As can be observed, the $MoSi_2$ particles are in contact with each other. It can be conceived that these particles are also spatially in contact with each other. Furthermore, the original sharp edges of $MoSi_2$ particles have been partially smoothed by the sintering process, which promotes an effective thermal contact between particles and favouring the occurrence of high conductive paths within the composite.

Since the thermal conductivity ratio between $MoSi_2$ and YPSZ is only about 20, the transition from insulating to conductive happens gradually; see Fig. 11a. This transition coincides with occurrence of percolation. Such a transition will be more abrupt when considering electrical conductivity; see details in [44].

The self-consistent model, however, represents well the heat conduction phenomena taking place in the dense YPZS-$MoSi_2$ composites across its entire composition range; see Fig. 11a. For low $MoSi_2$ volume fractions (less than 30%) the predictions by the SC and Bruggeman I model are very similar. With increasing volume fraction of $MoSi_2$, the SC model approaches the Bruggeman II model. Thus, the SC model accounts well for the occurrence of several percolation paths in the composites.

4.2. Porous YPSZ-$MoSi_2$ composites

Also, for porous composites it holds that the thermal diffusivity increases with the volume fraction of $MoSi_2$ particles; see Fig. 11b. The difference in size distribution of pores for dense and porous composites is shown in Fig. 12. The porous composites show rather coarser size distribution as compared to the dense composites.

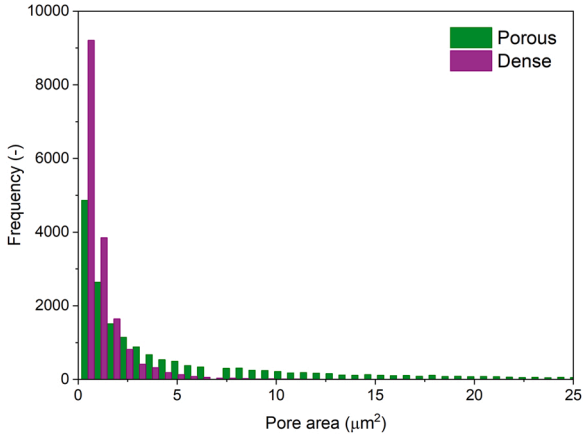

Fig. 12. Pore area distribution of typical dense and porous Yttria Partially Stabilized Zirconia (YPSZ) composites.

As for the dense composites, the Bruggeman I model is in a good agreement with the experimental data of the porous composites for volume fractions of $MoSi_2$ below 30%; see Fig. 11b. For volume fractions of $MoSi_2$ exciding 30%, the experimental thermal diffusivity of porous composites is somewhat larger than predicted by the Bruggeman I model, but less than expected according to the SC model. This is due to the sharp edges of highly conductive $MoSi_2$ particles, which are almost evenly surrounded by finer YPSZ particles and coarser pores; see Fig. 3 f. These factors are limiting the contact between the $MoSi_2$ particles even for high volumetric fractions. Thus, the occurrence of high conduction paths due to percolation of the $MoSi_2$ particles is less likely in the porous composites than in the dense composites.

The Bruggeman II model predicts the thermal diffusivity of porous composites significantly higher than the experimental values and those predicted by both Bruggeman I and SC models; see Fig. 11b. The SC and Bruggeman II model deliver similar predictions only when the volume fraction of $MoSi_2$ particles is more than 80%. This is due to the formation of several highly conductive paths through the thickness of the porous composite.

4.3. Comparison between dense and porous YPSZ-$MoSi_2$ composites

The thermal diffusivity of dense and porous YPSZ-$MoSi_2$ composites as a function of volume fraction of $MoSi_2$ show a similar behaviour; see Fig. 13. However, the thermal diffusivity of dense composites with a volume fraction of $MoSi_2$ less than 30% is larger than that of porous composites with the same $MoSi_2$ volume fraction; see the inset in Fig. 13. This is due to the more pronounced effect of the very low thermal conductivity of air within the pores as compared to the thermal conductivity of both YPSZ and $MoSi_2$; cf. Table 1. Thus, the effect of air on a mixture of solid materials is lowering the thermal conductivity of the composite. It should be noted that also the shape and the orientation of pores filled with air affects the thermal conductivity of the composite; see details in [35].

Nevertheless, the lowering effect of a fixed volume fraction of pores on the thermal diffusivity of a multiphase (when the number of phases is more than two) composite diminishes when the volume fraction of the high thermally conductive phase (i.e., $MoSi_2$) becomes large, as can be seen in Fig. 13. When considering $MoSi_2$ volume fractions larger than 30%, the experimental thermal diffusivity data of both dense and porous samples are almost indistinguishable, although no dense and porous

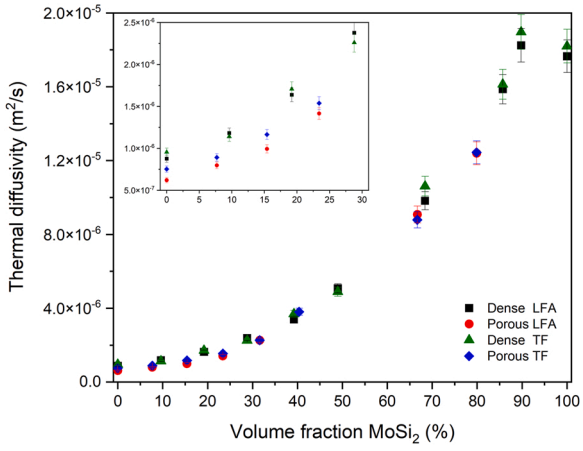

Fig. 13. Comparison between the thermal diffusivity of dense and porous Yttria Partially Stabilized Zirconia (YPSZ) composites versus the actual volume fraction of embedded $MoSi_2$ particles, as measured with Laser Flash Analysis (LFA) and Flash Thermography (FT).

samples with the same amount of $MoSi_2$ have been manufactured and tested in the frame of this work.

The explanation of this counterintuitive result is related to the double effect of pores on thermal diffusivity according to Eq. (2); namely: (*i*) the pores reduce thermal conductivity k_c of the composite and (*ii*) the pores reduce the overall thermal capacity of the composite, i.e., $\sum_{i=1}^{n} v_i \rho_i Cp_i$.

When pores do not effectively lower the thermal conductivity k_c (as for example for the in-parallel 1D model and for cylindrical and/or spherical pores [45]), it can happen that the thermal diffusivity of the porous samples is higher than the that of the dense samples with the same volume fraction of $MoSi_2$. This is due to the smaller overall thermal capacity of the porous composite than that of the dense composite.[1] However, when pores effectively lower the thermal conductivity k_c (as in the case of lamellar pores with the symmetry axis parallel to the heat flux or in the 1D in-series model [45]), the thermal diffusivity of porous composite is smaller than that of the corresponding dense composite.

This effect of the porosity on the thermal diffusivity and conductivity is displayed graphically in Fig. 14. The thermal conductivity and thermal diffusivity of the composite as a function of the $MoSi_2$ volume fraction are evaluated with both the 1D in-parallel and the SC model for dense and porous composites, respectively. As can be seen in Fig. 14, the thermal *conductivity* is similar for both type of composites (see Fig. 14a), while the thermal *diffusivity* of the porous composites is larger than that of dense composites (see Fig. 14b). In the case of the 1D in-parallel model, this occurrence takes place for every volumetric fraction of $MoSi_2$. Instead for the SC model thermal diffusivity of porous samples is higher than that of dense samples only for $MoSi_2$ volume fractions larger than 30% (see Fig. 14c). This happens because the effect of spherical pores in reducing thermal conductivity k_c is more pronounced than for the 1D in parallel model.

Thus, for the dense and porous composites studied in this work the net effect of the porosity on the thermal diffusivity is negligible when $MoSi_2$ volume fraction exceeds 30%; i.e., the thermal diffusivity for the dense and porous composites is the same.

5. Conclusions

The thermal diffusivity and conductivity of dense and porous binary composites having an insulating and conducting phases were studied across their entire composition range. Experimental evaluation has been performed with $MoSi_2$ particles embedded into yttria partially stabilized zirconia as prepared by spark plasma sintering. The thermal diffusivity of the composites increases with increasing volume fraction of $MoSi_2$. The thermal diffusivity of dense composites with a volume fraction of $MoSi_2$ less than 30% is larger than that of porous composites with the same volume fraction of $MoSi_2$. The effect of porosity on the thermal diffusivity of these composites diminishes for large volume fractions of $MoSi_2$.

The heat conduction of the dense YPSZ-$MoSi_2$ composites is accurately described with a self-consistent (SC) model, which captures the occurrence of high conduction percolation paths within the composite. In these composites the original sharp edges of $MoSi_2$ particles have been partially smoothed by the sintering process promoting an effective thermal contact between the embedded particles and favouring the occurrence of highly conductive paths inside the composites.

For porous YPSZ-$MoSi_2$ composites the Bruggeman I model describes adequately the heat conduction as a function of the volume fraction of $MoSi_2$. This is attributed to the sharp edges shape of $MoSi_2$ particles in the composite and a large volume fraction of pores limiting the occurrence of spatial highly conductive paths crossing the whole composite thickness.

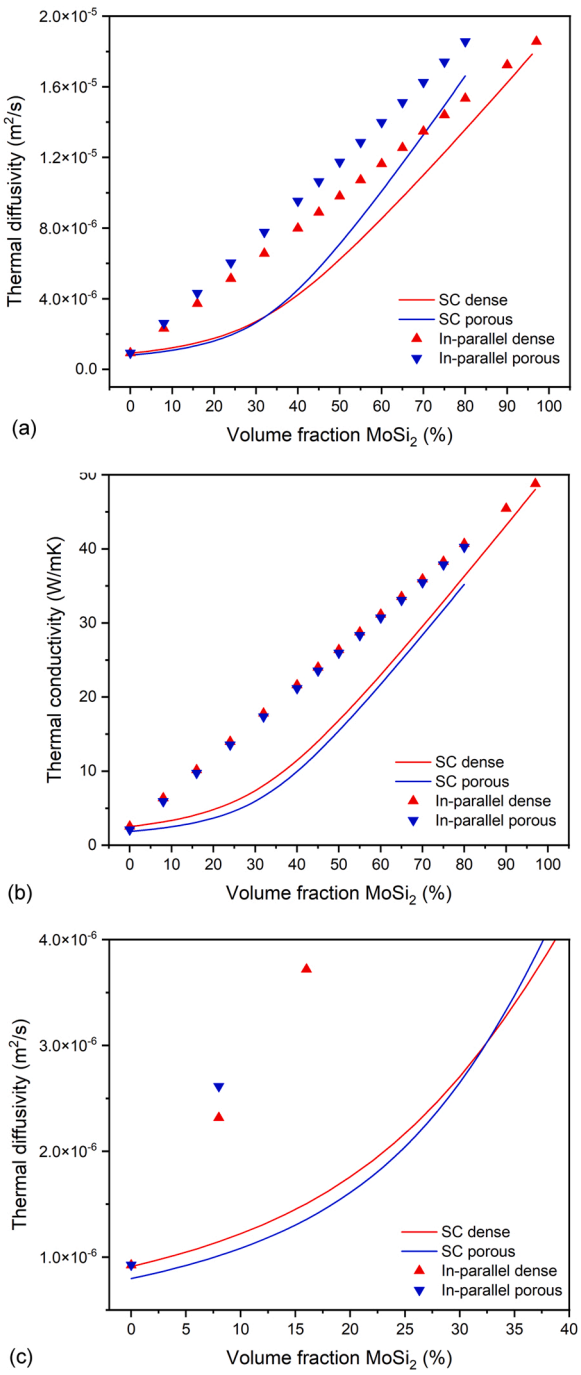

Fig. 14. (a) Thermal diffusivity of dense (3 vol.% porosity) and porous (20 vol.% porosity) Yttria Partially Stabilized Zirconia (YPSZ) composites versus the volume fraction of embedded $MoSi_2$ particles, as predicted by the Self-Consistent (SC) and 1D in-parallel model. (b) Thermal conductivity of dense (3 vol.% porosity) and porous (20 vol.% porosity) YPSZ composites versus the volume fraction of embedded $MoSi_2$ particles, as predicted by the Self-Consistent (SC) and 1D in-parallel model. (c) Enlargement of (a) at lower volume fractions of $MoSi_2$ shows the thermal diffusivity predicted by SC model for porous composites crosses the SC model for dense composites.

CRediT authorship contribution statement

Federico Cernuschi: Investigation, Formal analysis, Visualization, Writing – original draft. **Justyna Kulczyk-Malecka:** Investigation,

[1] Thisoccurrence is favored when the third phase (i.e., YPSZ) has a low thermalconductivity and a thermal capacity similar to that of the phase with highthermal conductivity (i.e., $MoSi_2$).

Formal analysis, Visualization, Writing – original draft. **Xun Zhang:** Experimental validation, Formal analysis, Writing – review & editing. **Franck Nozahic:** Experimental validation, Writing – review & editing. **Claude Estournès:** Experimental validation, Writing – review & editing. **Willem G. Sloof:** Conceptualization, Supervision, Resources, Project administration, Writing – review & editing.

Declaration of Competing Interest

The authors declare that they have no known competing financial interests or personal relationships that could have appeared to influence the work reported in this paper.

Acknowledgements

This project has received funding from European Union Seventh Framework Program (FP7/2007–2013) under grant agreement no. 309849, SAMBA. The authors thank A. L. Carabat and Z. Ding for assistance with the sample preparation. Justyna Kulczyk-Malecka is grateful to Andy Wallwork from University of Manchester for facilitating laser flash analysis.

References

[1] W.H. Tuan, Y.P. Pai, Mechanical properties of Al_2O_3-NiAl composites, J. Am. Ceram. Soc. 82 (6) (1999) 1624–1626.
[2] R.W. Rice, Mechanical properties of ceramics and composites: grain and particle effects, M. Dekker, New York, 2000, pp. 489–534.
[3] W.H. Tuan, Y.T. Chiu, Toughening alumina with metallic and zirconia inclusions, Key Eng. Mater. (1999) 337–340.
[4] J. Kulczyk-Malecka, X. Zhang, J. Carr, A.L. Carabat, W.G. Sloof, S. van der Zwaag, F. Cernuschi, F. Nozahic, D. Monceau, C. Estournes, P.J. Withers, P. Xiao, Influence of embedded $MoSi_2$ particles on the high temperature thermal conductivity of SPS produced yttria-stabilised zirconia model thermal barrier coatings, Surf. Coat. Tech. 308 (2016) 31–39.
[5] D.M. Liu, W.H. Tuan, Microstructure and thermal conduction properties of Al_2O_3-Ag composites, Acta Mater. 44 (2) (1996) 813–818.
[6] Y. Chen, X. Zhang, S. van der Zwaag, W.G. Sloof, P. Xiao, Damage evolution in a self-healing air plasma sprayed thermal barrier coating containing self-shielding $MoSi_2$ particles, J. Am. Ceram. Soc. (2019) 4899–4910.
[7] F. Nozahic, C. Estournès, A.L. Carabat, W.G. Sloof, S. van der Zwaag, D. Monceau, Self-healing thermal barrier coating systems fabricated by spark plasma sintering, Mater. Des. 143 (2018) 204–213.
[8]aa L. Boatemaa, S. van der Zwaag, W.G. Sloof, Self-healing of Al_2O_3 containing Ti microparticles, Ceram. Int. 44 (10) (2018) 11116–11126.
[9]ba L. Boatemaa, J.C. Brouwer, S. van der Zwaag, W.G. Sloof, The effect of the TiC particle size on the preferred oxidation temperature for self-healing of oxide ceramic matrix materials, J. Mater. Sci. 53 (8) (2018) 5973–5986.
[10]cbb L. Boatemaa, M. Bosch, A.S. Farle, G.P. Bei, S. van der Zwaag, W.G. Sloof, Autonomous high-temperature healing of surface cracks in Al_2O_3 containing Ti_2AlC particles, J. Am. Ceram. Soc. 101 (12) (2018) 5684–5693.
[11] S. Yoshioka, L. Boatemaa, S. van der Zwaag, W. Nakao, W.G. Sloof, On the use of TiC as high-temperature healing particles in alumina based composites, J. Eur. Ceram. Soc. 36 (16) (2016) 4155–4162.
[12] G.W. Lee, T.W. Kim, W.G. Sloof, K.S. Lee, Self-healing capacity of Mullite-Yb_2SiO_5 environmental barrier coating material with embedded Ti_2AlC MAX phase particles, Ceram. Int. 47 (16) (2021) 22478–22486.
[13] H.V. Pham, M. Nanko, W. Nakao, Self-Healing of Ni/Mullite hybrid materials via high-temperature oxidation, Mater. Trans. 58 (7) (2017) 1081–1088.
[14] D. Maruoka, M. Nanko, Recovery of mechanical strength by surface crack disappearance via thermal oxidation for nano-Ni/Al2O3 hybrid materials, Ceram. Int. 39 (3) (2013) 3221–3229.
[15] T. Osada, T. Hara, M. Mitome, S. Ozaki, T. Abe, K. Kamoda, T. Ohmura, Self-healing by design: universal kinetic model of strength recovery in self-healing ceramics, Sci. Technol. Adv. Mater. (2020) 593–608.
[16] P. Greil, Self-healing engineering ceramics with oxidation-induced crack repair, Adv. Eng. Mater. 22 (9) (2020) 1901121.
[17] W.H. Tuan, Design of multiphase materials, Key Eng. Mater. (2005) 963–966.
[18] D.A.G. Bruggeman, Berechnung verschiedener physikalischer Konstanten von heterogenen Substanzen. I. Dielektrizitätskonstanten und Leitfähigkeiten der Mischkörper aus isotropen Substanzen, Ann. der Phys. 416 (7) (1935) 636–664.
[19] L.E. Nielsen, Thermal conductivity of particulate-filled polymers, J. Appl. Polym. Sci. 17 (12) (1973) 3819–3820.
[20] L.E. Nielsen, The thermal and electrical conductivity of two-phase systems, Ind. Eng. Chem. Fundam. 13 (1) (1974) 17–20.
[21] A. Flaureau, A. Weibel, G. Chevallier, C. Estournès, Study of the densification and grain growth mechanisms occurring during spark plasma sintering of different submicronic yttria-stabilized zirconia powders, J. Eur. Ceram. Soc. 41 (6) (2021) 3581–3594.
[22] P. Scardi, M. Leoni, F. Cernuschi, A. Figari, Microstructure and heat transfer phenomena in ceramic thermal barrier coatings, J. Am. Ceram. Soc. 84 (4) (2001) 827–835.
[23] F. Cernuschi, P.G. Bison, A. Figari, S. Marinetti, E. Grinzato, Thermal diffusivity measurements by photothermal and thermographic techniques, Int. J. Thermophys. 25 (2) (2004) 439–457.
[24] F. Cernuschi, Can TBC porosity be estimated by non-destructive infrared techniques? A theoretical and experimental analysis, Surf. Coat. Technol. 272 (2015) 387–394.
[25] F. Cernuschi, P. Bison, Thirty years of thermal barrier coatings (TBC), photothermal and thermographic techniques: best practices and lessons learned, J. Therm. Spray. Technol. (2022).
[26] F. Cernuschi, P.G. Bison, S. Marinetti, P. Scardi, Thermophysical, mechanical and microstructural characterization of aged free-standing plasma-sprayed zirconia coatings, Acta Mater. 56 (16) (2008) 4477–4488.
[27] R.E. Taylor, K.D. Maglić, Compendium of thermophysical property measurement methods, in: Survey of measurement techniques, Vol. 1, Plenum Press, New York, 1984.
[28] R.E. Taylor, K.D. Maglić, Compendium of thermophysical property measurement methods, in: Recommended measurement techniques and practices, Vol. 2, Plenum Press, New York, 1992.
[29] I. Barin, Thermochemical Data of Pure Substances, VCH, Weinheim, 1995 (La-Zr).
[30] J. Leitner, P. Voňka, D. Sedmidubský, P. Svoboda, Application of Neumann–Kopp rule for the estimation of heat capacity of mixed oxides, Thermochim. Acta 497 (1) (2010) 7–13.
[31] T.B. Douglas, W.M. Logan, Heat Content of Molybdenum Disilicide from 0 to 900 °C, J. Res. Natl. Bur. Stand. 53 (2) (1954) 91–93.
[32] T. Tojo, T. Atake, T. Mori, H. Yamamura, Heat capacity and thermodynamic functions of zirconia and yttria-stabilized zirconia, J. Chem. Thermodyn. 31 (7) (1999) 831–845.
[33] Z. Wang, A. Kulkarni, S. Deshpande, T. Nakamura, H. Herman, Effects of pores and interfaces on effective properties of plasma sprayed zirconia coatings, Acta Mater. 51 (18) (2003) 5319–5334.
[34] M. Knudsen. The Kinetic Theory Of Gases: Some Modern Aspects, third ed., Methuen & Company, London, 1952.
[35] F. Cernuschi, P. Bison, A. Moscatelli, Microstructural characterization of porous thermal barrier coatings by laser flash technique, Acta Mater. 57 (12) (2009) 3460–3471.
[36] A. Zivelonghi, F. Cernuschi, C. Peyrega, D. Jeulin, S. Lindig, J.H. You, Influence of the dual-scale random morphology on the heat conduction of plasma-sprayed tungsten via image-based FEM, Comput. Mater. Sci. 68 (2013) 5–17.
[37] S. Torquato, Random Heterogeneous Materials: Microstructure and Macroscopic Properties, Springer, New York, 2002.
[38] G.W. Milton, The coherent potential approximation is a realizable effective medium scheme, Commun. Math. Phys. 99 (4) (1985) 463–500.
[39] R. Landauer, Electrical conductivity in inhomogeneous media, AIP Conference Proceedings, 1978, p. 2.
[40] R. Landauer, The electrical resistance of binary metallic mixtures, J. Appl. Phys. 23 (7) (1952) 779–784.
[41] E.H. Kennard. The Kinetic Theory of Gases. With an Introduction to Statistical Mechanics, first ed., McGraw-Hill Publishing Co., Ltd., London, 1938, pp. 60–74.
[42] D. Stauffer, A. Aharony. Introduction to Percolation theory, second ed., Taylor and Francis, London, 2003.
[43] S. Torquato, Modeling of physical properties of composite materials, Int. J. Solids Struct. 37 (1–2) (2000) 411–422.
[44] D.M. Liu, W.H. Tuan, Microstructure and its influence on thermal and electrical conductivity of ZrO_2-Ag composites, Mater. Chem. Phys. 48 (3) (1997) 258–262.
[45] F. Cernuschi, S. Ahmaniemi, P. Vuoristo, T. Mäntylä, Modelling of thermal conductivity of porous materials: application to thick thermal barrier coatings, J. Eur. Ceram. Soc. 24 (9) (2004) 2657–2667.
[46] David R. Lide, CRC Handbook of Chemistry and Physics, CRC Press/Taylor and Francis, Boca Raton, FL, USA, 2008, pp. 4–127 (ed.).